communications earth & environment

Article

A Nature Portfolio journal

https://doi.org/10.1038/s43247-025-02172-w

Thermochronological markers reveal Late Cretaceous strike-slip faulting in the Yangtze Block, South China

Xiaowei Zeng [1,2], Marco G. Malusà [2] ✉, Alberto Resentini [2], Yang Tian[3], Qingqing Lei[1] & Chuanbo Shen [1] ✉

Detecting strike-slip tectonics using thermochronology is challenging because the complex relative motion between fault blocks often does not substantially displace the vertical stratigraphy provided by thermochronological ages. Here we investigate the strike-slip tectonics in the Yangtze Block, South China, based on an original conceptual model and the zircon (U-Th)/He (ZHe) analysis of 17 sandstone samples. We exploit as a marker the northwestward trend of progressively decreasing ZHe ages generated by Mesozoic northwestward shortening. The ZHe age trend is broken by evident steps, which are also found in other published thermochronological datasets. We interpret these age steps as marking a previously undetected Late Cretaceous left-lateral strike-slip fault which intersects with prior deformation-propagation direction. Our approach to detect strike-slip faults confirms a major change in the subduction direction of the Paleo-Pacific Plate beneath Eurasia during the Late Cretaceous, and can find applications to other regions where thermochronological ages define suitable dipping markers.

Thermochronological data may provide useful markers to detect normal and reverse fault activity[1–4]. However, detecting strike-slip faults by thermochronological data is challenging. In most cases, the timing of strike-slip fault activity was constrained through identifying the vertical offset triggered by strike-slip movements, if recorded, in thermochronological data[5–7]. However, this approach has limitations because most thermochronological markers are insensitive to lateral displacements of fault blocks, while the vertical offset caused by strike-slip movements is complex and often of minor importance. In such scenarios, the thermochronological clocks on both sides of the fault do not record the strike-slip movements but rather the earlier thermal events. Nevertheless, these records could be regarded as virtual strata, which ought to be dissected by the lateral displacement caused by strike-slip movements, providing opportunities to constrain strike-slip faults. Progressive deformation during plate convergence may produce thermochronological age trends that are suitably oriented and can be used to reveal subsequent strike-slip faulting events, allowing us to test the above assumption in real geology.

The Eastern Sichuan-Xuefeng fold-and-thrust belt (ESXFTB) is a part of the Yangtze Block in South China, spanning from the Xuefeng Uplift in the east to the Sichuan Basin in the west[8] (Fig. 1a, b). It records the subduction of the Paleo-Pacific Plate underneath Eurasia during the Mesozoic[9,10] and provides an excellent natural laboratory for studying fold-and-thrust deformation in intracontinental orogenic belts[11]. Previous studies highlighted a northwestward progressive deformation affecting this fold-and-thrust belt during the Mesozoic[12–14] (Fig. 1c), which is responsible for the long-recognized trends of decreasing thermochronological ages from the SE to the NW[8,15,16]. These trends can be exploited as a marker to detect potential strike-slip movements in the subsequent stages of orogeny, in a region where tectonics is governed by varying Paleo-Pacific-Eurasia convergence directions[17] through time.

Despite strike-slip faults were locally described in the field within the ESXFTB[18,19], their role in this complex region is not fully assessed yet. To shed light on this issue, we present a dataset of 17 original ZHe ages. We exploit the regional thermochronological age pattern to reveal, and trace in map view, a large and previously undetected left-lateral strike-slip fault (Fig. 1b) and constrain its timing of deformation. The implications of the Late Cretaceous Paleo-Pacific Plate subduction pattern on intracontinental deformation are finally discussed.

Results

Geological settings

The ESXFTB is located in the central part of the Yangtze Block (Fig. 1a). Situated to the west of the Xuefeng uplift, it is marked by NW-directed

[1]Key Laboratory of Tectonics and Petroleum Resources, Ministry of Education, China University of Geosciences, Wuhan, 430074, China. [2]Department of Earth and Environmental Sciences, University of Milano-Bicocca, Milano, 20126, Italy. [3]School of Geosciences, Yangtze University, Wuhan, 430100, China.
✉e-mail: marco.malusa@unimib.it; cbshen@cug.edu.cn

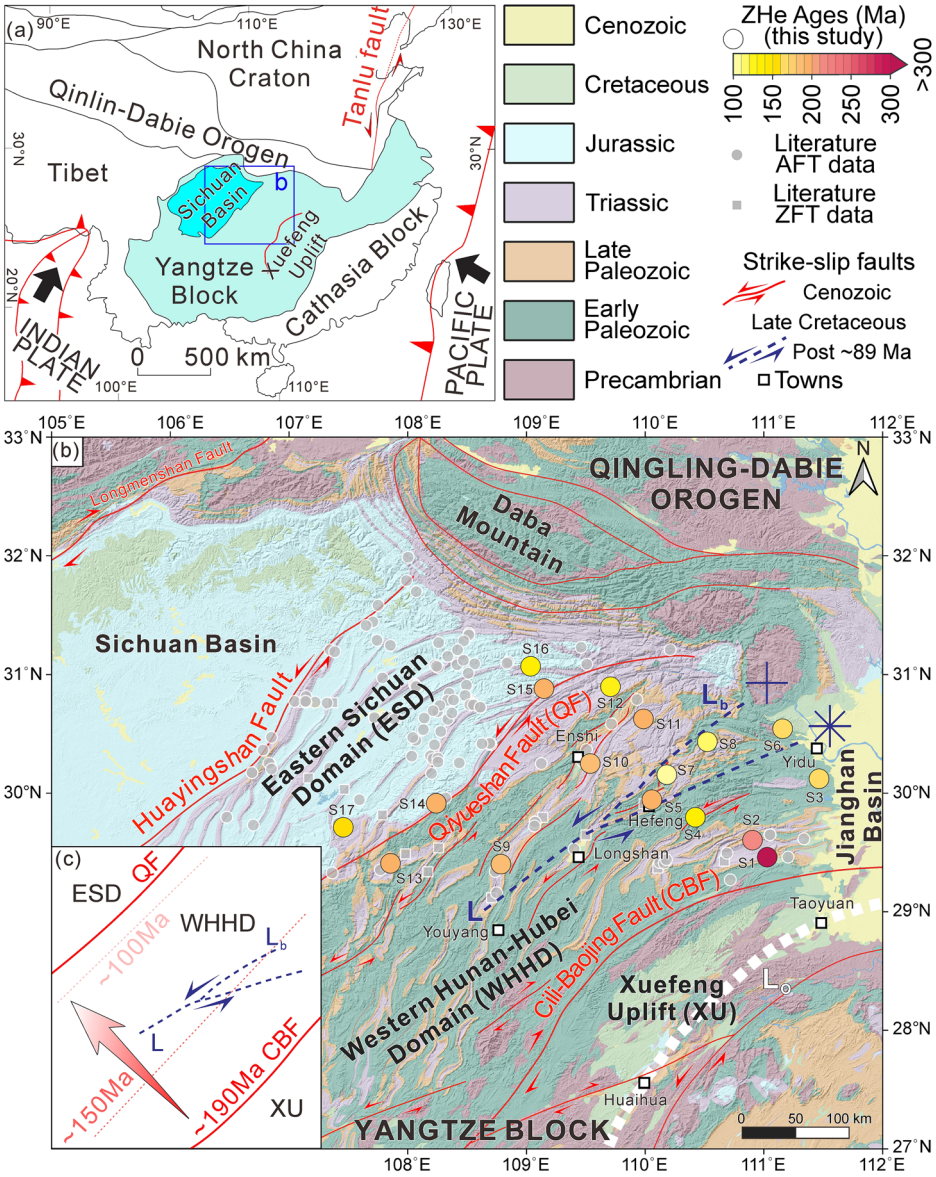

Fig. 1 | Geologic maps of the study region. **a** Simplified tectonic map of South China showing the location of the study area. The black arrows indicate Paleo-Pacific and India Plates motion. **b** Geologic map of the Eastern Sichuan-Xuefeng fold-and-thrust belt. Cenozoic faults (in red) after Wang et al.[18]. The blue dashed line L and its branch L_b represent the strike-slip fault revealed in this study. The asterisk and cross represent L and L_b, respectively. Line L_O represents the initial front of regional Mesozoic deformation derived from the restorations of balanced cross sections[16]. **c** Model of progressive deformation propagation (red arrow, time in Ma) within the study area according to analogue modelling results[14]. XU, Xuefeng Uplift; WHHD, Western Hunan-Hubei Domain; ESD, Eastern Sichuan Domain. The red solid lines indicate the Cili-Baojing (CBF) and Qiyueshan (QF) Faults. The reddish dotted lines and associated time represent the approximate location and timing of the regional Mesozoic deformation. Image generated using Qgis 3.36.2 (https://qgis.org/en/site/) and Inkscape 1.3 (https://inkscape.org).

thrusts, nappes, and NE-NNE-striking arcuate structures. It stretches from the Cili-Baojing Fault in the SE to the Huayingshan Fault in the NW, divided by the Qiyueshan Fault into the Western Hunan-Hubei Domain and the Eastern Sichuan Domain (Fig. 1b).

During the Mesozoic, the ESXFTB underwent northwestward-propagating deformation[8,12], which began in the Late Triassic[11,20] and proceeded northwestward from the Early Jurassic to Late Cretaceous[13,15] due to the continued subduction of the Paleo-Pacific Plate beneath Eurasia. The Mesozoic progressive deformation is confirmed by thermal history reconstructions based on apatite fission-track (AFT) data[15,16] and the decreasing number of Mesozoic unconformities northwestward[21]. Although dominated by thrust structures, the ESXFTB also underwent strike-slip movements since the Late Cretaceous (Fig. 1b), which were also documented in the adjacent Yuanma Basin within the Xuefeng Uplift[22,23]. However, the timing of those strike-slip faults remains poorly constrained due to the lack of Mesozoic stratigraphic record[19,24] (Fig. 1b). The northwestward-decreasing trends of apatite and zircon fission-track ages[16,20] (ZFT) generated during regional progressive deformation in the Mesozoic may provide suitable thermochronological markers to reveal younger strike-slip faults. However, AFT ages are mainly Late Cretaceous or younger, whereas ZFT ages are mainly Late Triassic. They do not cover the main deformation stages revealed by AFT thermal history modeling[15], and no major age break in the AFT and ZFT map-view distribution patterns was highlighted by previous studies. The ZHe system, having a partial retention zone in between the partial annealing zones of the AFT and ZFT systems[25], may provide a useful tool to unravel the puzzle of Mesozoic deformation within the central Yangtze Block and reveal subsequent strike-slip faulting during the Late Cretaceous and beyond.

ZHe ages confirm primary Mesozoic deformation

Weighted mean ZHe ages are shown in Fig. 2a and mainly fall between the Late Triassic and the Late Cretaceous. Single-grain ZHe ages that are older than the corresponding stratigraphic ages were excluded to avoid biasing the dataset, and the derived age trends, with unreset or overcorrected ages (see Methods for details on data filtering). Kernel density estimates (KDE) of single-grain ZHe ages are reported in Fig. 2b (see Supplementary Tables 1 and 2 for ZHe data). Literature AFT and ZFT data are summarized in Fig. 2c (Supplementary Tables 3 and 4). AFT, ZFT, and ZHe ages are plotted in Fig. 2a, c versus their distance from the initial front of regional Mesozoic deformation, derived from the restorations of balanced cross sections[16] (line L_O in Fig. 1b), which passes through the towns of Huaihua and Taoyuan and is parallel to the trend of the Xuefeng uplift. From the

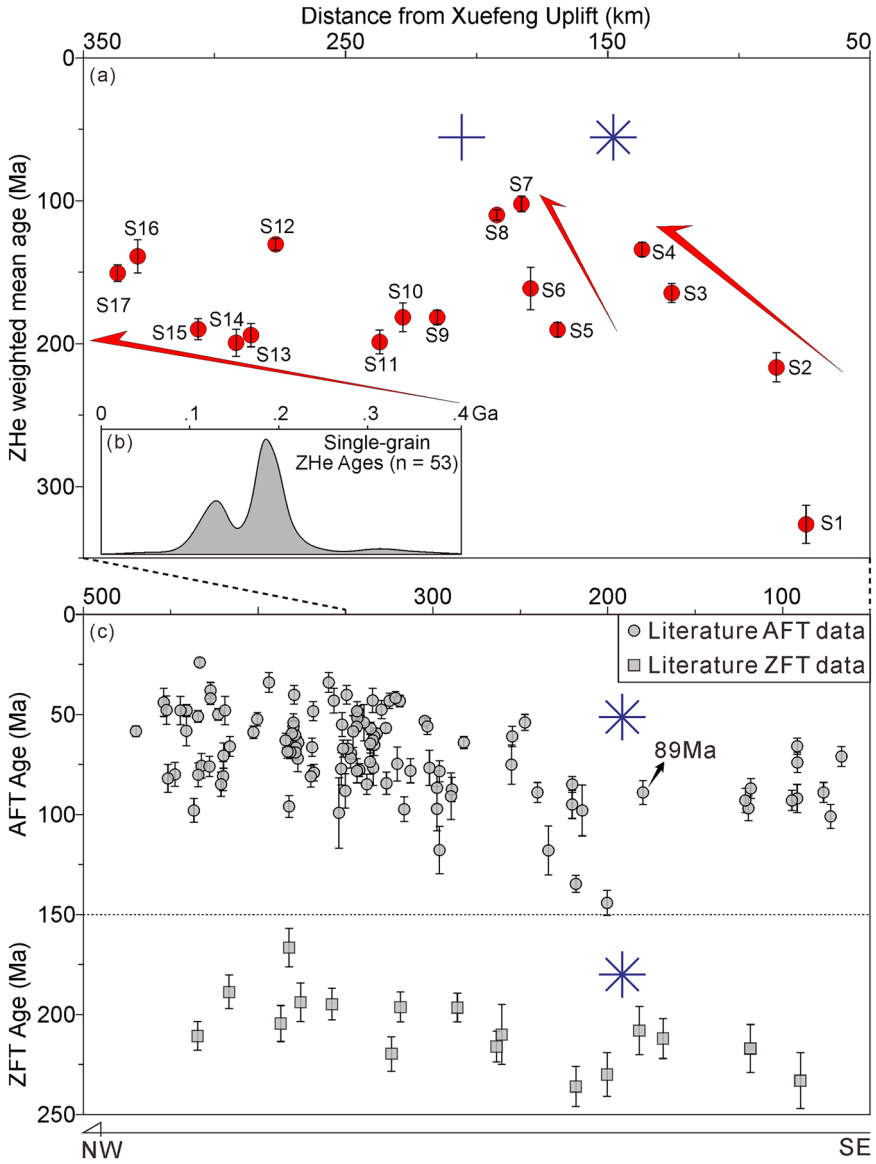

Fig. 2 | ZHe data and published AFT, ZFT data. **a** Reset ZHe weighted mean ages versus sample distance from the regional Mesozoic deformation initial front (L_O in Fig. 1b). Blue asterisk and cross indicate the main age breaks marking the strike-slip fault detected in this study (L and L_b in Fig. 1b). The red arrows show the observed age trends. Error bars indicate ±1 s.e. **b** Kernel density estimate of all accepted single grain ZHe ages. **c** AFT and ZFT ages versus distance from L_O (Fig. 1b). Blue asterisks mark the location of strike-slip fault L. Image generated using IsoplotR[49] and Inkscape 1.3 (https://inkscape.org).

Xuefeng Uplift to the Eastern Sichuan Domain, ZHe data indicates a general northwestward trend of decreasing ages (Fig. 2a), which confirms the two trends delineated by AFT and ZFT ages (Fig. 2c). All AFT ages are younger than the corresponding stratigraphic ages (Fig. 2c and Supplementary Table 3), indicating that the samples have been reset due to burial after deposition. The same applies to ZFT ages (Fig. 2c and Supplementary Table 4). The observed distribution for ZHe ages (Fig. 2a) systematically falls between the ranges observed for AFT and ZFT ages, as expected for thermochronological ages that record exhumation[25]. A few single-grain ZHe ages from the Jurassic strata overlap within error with the stratigraphic age, which might suggest the presence of magmatic-age components. However, these ZHe ages are younger than the youngest ZFT age component observed in the same strata[20,26], which rules out any major impact of volcanic activity on the observed ZHe age trends. This is consistent with the observation that the study area lacks Mesozoic magmatic activity, which was confined, in South China, to the east of the Xuefeng Uplift during the Mesozoic[27].

Left-lateral strike-slip fault detected by age breaks

Evident breaks are found in the ZHe age trend from younger to older ZHe ages, which are indicated by blue markers in Fig. 2a. Similar age breaks are also found in the AFT and ZFT age trends (asterisk in Fig. 2c). The locations of these breaks in map view define a branched line indicated in blue in Fig. 1b (L and its branch L_b). Ages suddenly become older when crossing the line, then restart the northwestward decreasing age trend on the western side of the line.

The reason for the observed age break is explained in the conceptual model of Fig. 3. In our interpretation, line L, together with its branch L_b represents an undetected left-lateral strike-slip fault, referred to as the Yidu-Hefeng branched strike-slip fault hereafter. The Yidu-Hefeng Fault juxtaposes rocks with old ZHe ages on the NW block to rocks with young ZHe ages on the SE block. This is because the original trend of decreasing ZHe ages generated by Mesozoic deformation was cut obliquely by this left-lateral strike-slip fault, which divided the region into two blocks with partly overlapping ZHe ages. After left-lateral strike-slip, the youngest ages in the SE block are found in contact with the oldest ages in the NW block (Fig. 3).

The conceptual model of Fig. 3 also explains other major features revealed by our analysis. They are the trend of progressively older ages from the SW to the NE observed on the northern block of the L fault (Fig. 1b), and the occurrence of two age peaks, in the Early Jurassic (~180 Ma) and in the Early Cretaceous (~ 125 Ma), observed in the KDE of Fig. 2b. A trend of progressively older ages is indeed predicted by our conceptual model moving parallel to the fault (from the left to the right in Fig. 3). And the fact that the KDE is polymodal, despite the starting age distribution being more gradual, is a direct effect of the repetition in outcrops of rocks characterized by a similar thermochronological imprint on the opposite sides of the fault

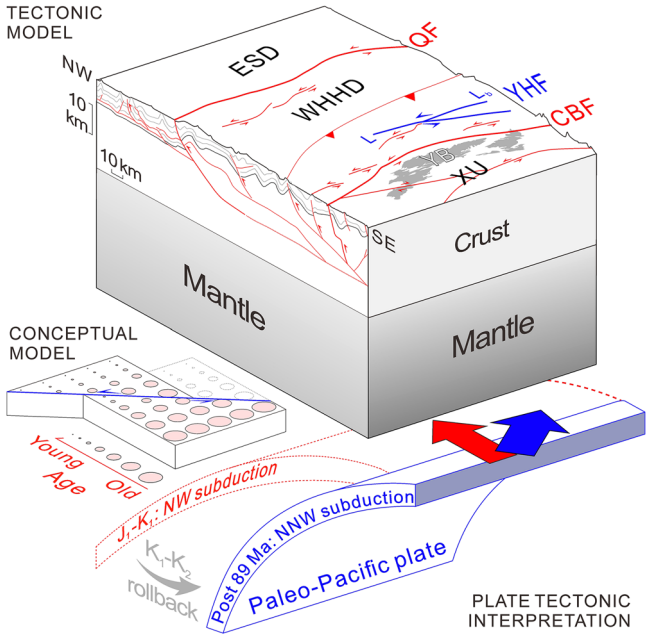

Fig. 3 | Conceptual and tectonic models. The conceptual model on the left illustrates how left-lateral strike-slip faulting produces age breaks in pre-existing thermochronological age trends. The tectonic model and plate tectonic interpretation show the orogenic belt caused by NW subduction of the Paleo-Pacific Plate since the Early Jurassic (geological cross-section after Dong et al[51].), basin formation during slab rollback in the Cretaceous, and the activation of the Yidu-Hefeng strike-slip fault after the change of subduction direction in the Late Cretaceous. XU, Xuefeng Uplift; YB, Yuanma Basin; CBF, Cili-Baojing Fault; YHF, Yidu-Hefeng branched strike-slip Fault (L and its branch L_b); WHHD, Western Hunan-Hubei Domain; ESD, Eastern Sichuan Domain. Image generated using Inkscape 1.3 (https://inkscape.org).

(Fig. 3). These repeated ages, being more represented in the distribution, determine peaks where a more gradual distribution would have been expected.

Obviously, only trends generated before faulting are offset. Therefore, the Yidu-Hefeng Fault was necessarily active after the youngest displaced age was set. This is the 89 Ma AFT age shown in Fig. 2c, which is supportive of fault activity starting not earlier than the Late Cretaceous. Previous regional geological studies have revealed several NE to ENE small-scale and discontinuous left-lateral faults in the study region. Some authors have interpreted these faults within the framework of a NE-SW zone of distributed right-lateral shear accommodating India-Asia convergence during the Cenozoic[18]. However, the location of these Cenozoic strike-slip faults (in red in Fig. 1b) does not fit with the location of the faults revealed by thermochronological age breaks, despite the orientation being virtually the same.

Discussion

The activation of the Yidu-Hefeng strike-slip fault detected in this work is interpreted in the light of the Late Cretaceous evolution of the Paleo-Pacific subduction zone. As shown in the tectonic model in Fig. 3, the progressive deformation within the ESXFTB was likely triggered by the subduction of the Paleo-Pacific Plate since the Early Jurassic[28] and the formation of a regional large-scale fold-and-thrust belt in the Jurassic – Early Cretaceous (in red in Fig. 3) as recorded by ZHe ages. This event is extensively documented across South China and includes magmatic intrusions east of the Xuefeng Uplift during the Early Jurassic[9,27,29], the widespread development of NE-directed thrust faults[12], and large-scale copper, lead-zinc, and tungsten mineralizations[30].

A major tectonic change took place in the Cretaceous due to the rollback of the Paleo-Pacific Plate (in grey in Fig. 3), which resulted in extensive magmatic activity across East Asia[10,31], especially in the Cathasia Block, accompanied by formation of ore deposits[32–34] and sedimentary basins[21,35] as evidenced in the Xuefeng Uplift[23]. By utilizing the age decreasing trends in regional thermochronological datasets, a previously undetected left-lateral strike-slip fault is revealed at this stage. Its onset time is after ~89 Ma, as constrained by the AFT data (Fig. 2c). We interpret the left-lateral strike-slip in the light of a change of convergence direction between Eurasia and the Paleo-Pacific Plate, from NW-SE to around N-S (Fig. 3). The change in subduction direction of the Paleo-Pacific Plate[31] triggered left-lateral strike-slip motion along the entire Tanlu Fault[36] (~97–82 Ma, Fig. 1a), and also induced widespread transpression in the South China Block[17]. Notably, the ESXFTB hosts several strike-slip faults that were active since the Late Cretaceous[18,19] (Fig. 1b). The western Xuefeng Uplift experienced major transpression and left-lateral slip during the Late Cretaceous[23,37], when exhumation revealed by AFT analysis led to the cessation of hydrocarbon generation[38] and to the influx of meteoric water with further shale gas dispersion in the study area[39].

The activity of the Yidu-Hefeng strike-slip fault necessarily precedes the main stages of Indo-Asian collision (~ 50Ma[40,41]), because India-Eurasia convergence is expected to produce right-lateral strike-slip tectonics in the Yangtze Block, as documented for example within the Western Hunan-Hubei Domain and in the Sichuan Basin[18,42], not left-lateral strike-slip tectonics as observed in the ESXFTB. Geologic maps of the eastern margin of the Sichuan Basin show a general S-shaped folding pattern, which originates from Early Cretaceous NE-trending linear folds that have been subsequently deformed within a framework of distributed NE-SW right-lateral shear. The minimum age of right-lateral shear is constrained to the Cenozoic, coeval with Indo-Asian collision[18,42]. The major post 89 Ma NE-SW left-lateral strike-slip documented in this study was thus concluded before the onset of distributed NE-SW right-lateral shearing described by Wang et al.[18].

Thermochronology age breaks across strike-slip faults are common in nature, as evidenced by examples in the Alps[43], Tibet[44], and Tianshan[45]. Although these age breaks could be attributed to differential exhumation across faults[44,45], our case study suggests that they can also result from the horizontal displacement of fault blocks if the thermochronological signals induced by earlier regional thermal events are not reset. We suggest taking this effect into careful consideration when reconstructing thermal histories and calculating exhumation rates of strike-slip fault blocks, because age offsets caused by horizontal displacement may have a major impact on thermal modeling. This is particularly important in the light of the capability of the latest version of modeling software such as QTQt, which offers thermochronologists the capability to perform regional planar thermal history inversion models[46]. This advancement raises the bar for understanding the impact of planar deformation on the spatial distribution patterns of thermochronological ages.

In conclusion, we successfully use thermochronological markers and a simple conceptual model to reveal an undetected strike-slip fault and constrain its onset time. Our ZHe thermochronology data record the northwestward propagating deformation within the central Yangtze Block, which is caused by the NW subduction of the Paleo-Pacific Plate during the Early Jurassic to the Late Cretaceous. Together with previous AFT and ZFT datasets, regional thermochronological datasets collectively reveal a major left-lateral strike-slip fault and limit its onset time after ~89 Ma. Strike-slip motion requires a change in the regional compression direction during the Late Cretaceous, which is likely controlled by the change of subduction direction of the Paleo-Pacific Plate beneath Eurasia. Our results provide evidence for the Paleo-Pacific Plate subduction evolution during the Late Cretaceous and reflect the impact of plate subduction processes on intracontinental tectonic deformation, confirming the potential of thermochronology in studying the relationships between surface processes in complex geodynamic environments.

Methods

Zircon (U-Th)/He

We collected 17 sandstone samples for ZHe analysis across the ESXFTB (Supplementary Table 1), from strata ranging in age between the Upper

Paleozoic and the Upper Cretaceous. Samples were crushed and processed with standard magnetic and density separation methods[25] to retrieve zircon grains for analysis. U and Th isotopic ratios were measured in the Thermochronology Lab at the University of Florida. Zircon crystals free of impurities, inclusions, and fractures were selected under a stereomicroscope, and their dimensions were measured to calculate alpha-ejection corrections[47]. Grains were encapsulated in Nb tubes, degassed with a diode laser, and heated at least twice (each heating process lasted 20 minutes at 9 Amp) for complete helium extraction. The extracted gas, mixed with >99.99% pure ^{3}He spike, underwent purification with an NP-10 getter. ^{4}He/^{3}He ratios were measured with a Pfeiffer-Blazers Prisma quadrupole mass spectrometer after a two-minute equilibration. Degassed zircon packets were then spiked, and bomb-dissolved using strong acids of HNO_3, HF, and HCl, and their U and Th isotopic ratios were measured by Thermo-Finnigan Element2 ICP-MS. Fish Canyon Tuff zircon served as age standards. Single grain ZHe ages are listed in Supplementary Table 2.

Data reduction and distance calibration

We performed data filtering and abandoned single-grain ZHe ages older than the stratigraphic deposition age to avoid bias in the analyzed age trends related to overcorrected or unreset ages. Although some single-grain ZHe ages from the Jurassic strata coincided with the stratigraphic deposition age after filtering, all these ages remained younger than the provenance-related ZFT age components from the same strata, with the minimum age being 216 Ma[20]. One grain in sample S4 yielded an age of 58.1 ± 1.4 Ma which is much younger than other grains in this sample and previous AFT ages in this area (within Western Hunan-Hubei Domain, Fig. 1b and Supplementary Table 2). Considering the partial annealing zone of AFT is usually lower than the partial retention zone of ZHe, this grain is regarded as an outlier and thus ignored. In particular, the eU of this grain is higher than that of other grains in the same sample, and there is no evidence of major reheating around ~58 Ma in the study area that could cause the zircon (U-Th)/He partial retention zone to fall below the AFT partial annealing zone[48]. This further supports our decision to consider this age as an outlier. The weighted mean ages of reset ZHe grains for all samples were calculated using IsoPlotR software[49]. Published AFT and ZFT data are collected and listed in Supplementary Tables 3 and 4. Only outcrop sample data were collected. Unreset ages are ignored following the procedure as in ZHe data processing to avoid effect of distant source thermal history.

All samples location were imported into QGIS. Their distance from the regional Mesozoic deformation initial front line, i.e. the L_O in Fig. 1b, were calculated with Nearest neighbor algorithm by NNjoin plugin (version 3.1.3) in QGIS software (version 3.28.8).

Data availability

Zircon (U-Th)/He data and collected thermochronological data are included in the supplementary information file and are also accessible via https://doi.org/10.6084/m9.figshare.28329260. The 3 Arc Shuttle Radar Topography Mission DEM data used for geological map in the study are available at CGIAR CSI SRTM 90 m DEM Digital Elevation Database via http://srtm.csi.cgiar.org/[50]. The regional lithology data shown in Fig. 1b are available at Geoscientific Data & Discovery Publishing System via http://dcc.ngac.org.cn/[19].

Code availability

IsoplotR software used for ZHe weighted mean ages calculation and KDE plot (Fig. 2a, b) is available via Vermeesch (2018)[49]. Version 3.36.2 of QGIS software used for geological map processing is available via https://qgis.org/en/site/. Version 3.1.3 of QGIS plugin NNjoin used for distance calculation between samples and the regional Mesozoic deformation initial front line, i.e. the L_O in Fig. 1b, is available via https://plugins.qgis.org/plugins/NNJoin/. All figures were drawn and finalized using Inkscape version 1.3 (https://inkscape.org/).

Received: 22 July 2024; Accepted: 26 February 2025;
Published online: 08 March 2025

References

1. Ault, A. K., Reiners, P. W., Evans, J. P. & Thomson, S. N. Linking hematite (U-Th)/He dating with the microtextural record of seismicity in the Wasatch fault damage zone, Utah, USA. *Geology* **43**, 771–774 (2015).
2. McDermott, R. G., Ault, A. K. & Caine, J. S. Dating fault damage along the eastern Denali fault zone with hematite (U-Th)/He thermochronometry. *Earth Planet. Sci. Lett.* **563**, 116872 (2021).
3. Tagami, T. Application of Fission-Track Thermochronology to Understand Fault Zones. in *Fission-Track Thermochronology and its Application to Geology* (eds. Malusà, M. G. & Fitzgerald, P. G.) 221–233 (Springer, Cham, 2019).
4. Tagami, T. Thermochronological investigation of fault zones. *Tectonophysics* **538–540**, 67–85 (2012).
5. Duvall, A. R. et al. Low-temperature thermochronometry along the Kunlun and Haiyuan Faults, NE Tibetan Plateau: Evidence for kinematic change during late-stage orogenesis. *Tectonics* **32**, 1190–1211 (2013).
6. Tadayon, M. et al. The Post-Eocene Evolution of the Doruneh Fault Region (Central Iran): The Intraplate Response to the Reorganization of the Arabia-Eurasia Collision Zone. *Tectonics* **36**, 3038–3064 (2017).
7. Benowitz, J. A. et al. Spatial variations in focused exhumation along a continental-scale strike-slip fault: The Denali fault of the eastern Alaska Range. *Geosphere* **7**, 455–467 (2011).
8. Zhou, C. & Zhou, J. Relationship Between Lateral/Basal Shear Stress Ratio and Structural Vergence of Thrust Wedges: Results From Analogue Modeling and Implications for the Origin of Eastern Sichuan–Xuefeng Fold-Thrust Belt in South China. *Tectonics* **41**, e2021TC007035 (2022).
9. Tao, N. et al. Post-250 Ma thermal evolution of the central Cathaysia Block (SE China) in response to flat-slab subduction at the proto-Western Pacific margin. *Gondwana Res.* **75**, 1–15 (2019).
10. Li, Z. & Li, X. Formation of the 1300-km-wide intracontinental orogen and postorogenic magmatic province in Mesozoic South China: A flat-slab subduction model. *Geology* **35**, 179–182 (2007).
11. Zhang, G. et al. Tectonics of South China continent and its implications. *Sci. China Earth Sci.* **56**, 1804–1828 (2013).
12. Li, S., Santosh, M., Zhao, G., Zhang, G. & Jin, C. Intracontinental deformation in a frontier of super-convergence: A perspective on the tectonic milieu of the South China Block. *J. Asian Earth Sci.* **49**, 313–329 (2012).
13. Yan, D., Zhou, M., Song, H., Wang, X. & Malpas, J. Origin and tectonic significance of a Mesozoic multi-layer over-thrust system within the Yangtze Block (South China). *Tectonophysics* **361**, 239–254 (2003).
14. He, W., Zhou, J. & Yuan, K. Deformation evolution of Eastern Sichuan–Xuefeng fold-thrust belt in South China: Insights from analogue modelling. *J. Struct. Geol.* **109**, 74–85 (2018).
15. Feng, Q., Qiu, N., Wu, H. & Koyi, H. Thermo-Kinematic Constraints on Restoration of the Eastern Sichuan Fold-And-Thrust Belt, South China. *Tectonics* **42**, e2022TC007630 (2023).
16. Mei, L., Liu, Z., Tang, J., Shen, C. & Fan, Y. Mesozoic intra-continental progress deformation in western Hunan-Hubei-Eastern Sichuan Province of China: Evidence from apatite fission track and balanced cross-section. *Earth Sci.* **35**, 161–174 (2010).
17. Wang, Y., Fan, W., Zhang, G. & Zhang, Y. Phanerozoic tectonics of the South China Block: Key observations and controversies. *Gondwana Res.* **23**, 1273–1305 (2013).
18. Wang, E. et al. Block rotation: Tectonic response of the Sichuan basin to the southeastward growth of the Tibetan Plateau along the Xianshuihe-Xiaojiang fault. *Tectonics* **33**, 686–718 (2014).
19. Li, C. et al. China national digital geological map (public version at 1:200 000 scale) spatial database. *Geol. China* **46**, 1–10 (2019).

20. Zheng, C., Xu, C., Brix, M. R. & Zhou, Z. Evolution and provenance of the Xuefeng intracontinental tectonic system in South China: Constraints from detrital zircon fission track thermochronology. *J. Asian Earth Sci.* **176**, 264–273 (2019).
21. Li, S. et al. Mesozoic tectono-magmatic response in the East Asian ocean-continent connection zone to subduction of the Paleo-Pacific Plate. *Earth-Sci. Rev.* **192**, 91–137 (2019).
22. Li, J., Zhang, Y., Dong, S. & Johnston, S. T. Cretaceous tectonic evolution of South China: A preliminary synthesis. *Earth-Sci. Rev.* **134**, 98–136 (2014).
23. Li, J., Zhang, Y., Dong, S. & Li, H. Late Mesozoic–Early Cenozoic deformation history of the Yuanma Basin, central South China. *Tectonophysics* **570–571**, 163–183 (2012).
24. BGMR (Bureau of Geology and Mineral Resources) of Hunan Province. *Regional Geology of the Hunan Province*. (Geological Publishing House, Beijing, 1988).
25. Malusa, M. G. & Fitzgerald P. G. (Eds.). *Fission-Track Thermochronology and Its Application to Geology*. (Springer, Cham, 2019).
26. Zheng C. Fission-track analyses for the tectonothermal history of eastern Sichuan basin in Mesozoic. Ph. D thesis. (Tongji University, Shanghai, 2020).
27. Cao, X., Flament, N., Li, S. & Müller, R. D. Spatio-temporal evolution and dynamic origin of Jurassic-Cretaceous magmatism in the South China Block. *Earth-Sci. Rev.* **217**, 103605 (2021).
28. Li, Y. et al. Late Jurassic to early Early Cretaceous tectonic nature on the NE Asian continental margin: Constraints from Mesozoic accretionary complexes. *Earth-Sci. Rev.* **200**, 103042 (2020).
29. Tao, N. et al. Thermochronological record of Middle–Late Jurassic magmatic reheating to Eocene rift-related rapid cooling in the SE South China Block. *Gondwana Res.* **46**, 191–203 (2017).
30. Mao, J., Xie, G., Li, X., Zhang, C. & Wang, Y. Mesozoic Large-scale Mineralization and Multiple Lithospheric Extensions in South China. *Acta Geol. Sin. - Engl. Ed.* **80**, 420–431 (2006).
31. Wang, F. et al. Temporal changes in the subduction of the Paleo-Pacific plate beneath Eurasia during the late Mesozoic: Geochronological and geochemical evidence from Cretaceous volcanic rocks in eastern NE China. *Lithos* **326–327**, 415–434 (2019).
32. Zeng, Y. et al. Prolonged Mesozoic intracontinental gold mineralization in the South China Block controlled by lithosphere architecture and evolving Paleo-Pacific Plate subduction. *Earth-Sci. Rev.* **240**, 104387 (2023).
33. Cai, W. et al. Zircon U–Pb and molybdenite Re–Os geochronology and geochemistry of Jinchang porphyry gold–copper deposit, NE China: Two-phase mineralization and the tectonic setting. *Ore Geol. Rev.* **107**, 735–753 (2019).
34. Dai, J. et al. Origin of the Woxi orogenic Au-Sb-W deposit in the west Jiangnan Orogen of South China: Constraints from apatite and wolframite U-Pb dating and pyrite in-situ S-Pb isotopic signatures. *Ore Geol. Rev.* **150**, 105134 (2022).
35. Li, J. et al. Cretaceous long-distance lithospheric extension and surface response in South China. *Earth-Sci. Rev*. 104496 (2023).
36. Yin, H. et al. Continental response to mid-Cretaceous global plate reorganization: Evidence from the Tan–Lu Fault Zone, eastern China. *Gondwana Res.* **86**, 23–45 (2020).
37. Tang, S., Yan, D., Qiu, L., Gao, J. & Wang, C. Partitioning of the Cretaceous Pan-Yangtze Basin in the central South China Block by exhumation of the Xuefeng Mountains during a transition from extensional to compressional tectonics? *Gondwana Res.* **25**, 1644–1659 (2014).
38. Ge, X., Shen, C., Selby, D., Deng, D. & Mei, L. Apatite fission-track and Re-Os geochronology of the Xuefeng uplift, China: Temporal implications for dry gas associated hydrocarbon systems. *Geology* **44**, 491–494 (2016).
39. Fan, Q. et al. In situ U-Pb dating of carbonate veins in Cambrian shales constrains fluid flow and hydrocarbon evolution at the southeastern margin of the Upper Yangtze platform, southwestern China. *GSA Bull*. **136**, 2875–2890 (2023).
40. Wang, X. et al. Cenozoic pulsed deformation history of northeastern Tibetan Plateau reconstructed from fission-track thermochronology. *Tectonophysics* **672–673**, 212–227 (2016).
41. van Hinsbergen, D. J. J., Steinberger, B., Doubrovine, P. V. & Gassmöller, R. Acceleration and deceleration of India-Asia convergence since the Cretaceous: Roles of mantle plumes and continental collision. *J. Geophys. Res. Solid Earth* **116**, B06101 (2011).
42. Tong, Y. et al. Passive crustal clockwise rotational deformation of the Sichuan Basin since the Miocene and its relationship with the tectonic evolution of the fault systems on the eastern edge of the Tibetan Plateau. *GSA Bull.* **131**, 175–190 (2019).
43. Malusà, M. G., Polino, R. & Zattin, M. Strain partitioning in the axial NW Alps since the Oligocene. *Tectonics* **28**, TC3005 (2009).
44. Ansberque, C. et al. Differential Exhumation Across the Longriba Fault System: Implications for the Eastern Tibetan Plateau. *Tectonics* **37**, 663–679 (2018).
45. Wang, Y., Zhang, J., Huang, X. & Wang, Z. Cenozoic exhumation of the Tianshan as constrained by regional low-temperature thermochronology. *Earth-Sci. Rev.* **237**, 104325 (2023).
46. Gallagher, K. Transdimensional inverse thermal history modeling for quantitative thermochronology. *J. Geophys. Res. Solid Earth* **117**, B02408 (2012).
47. Farley, K. A., Wolf, R. A. & Silver, L. T. The effects of long alpha-stopping distances on (U-Th)/He ages. *Geochim. Cosmochim. Acta* **60**, 4223–4229 (1996).
48. Gérard, B. et al. Zircon (U-Th)/He Closure Temperature Lower Than Apatite Thermochronometric Systems: Reconciliation of a Paradox. *Minerals* **12**, 145 (2022).
49. Vermeesch, P. IsoplotR: A free and open toolbox for geochronology. *Geosci. Front.* **9**, 1479–1493 (2018).
50. Reuter, H. I., Nelson, A. & Jarvis, A. An evaluation of void-filling interpolation methods for SRTM data. *Int J Geogr Inf Sci.* **9**, 983–1008 (2007).
51. Dong, S. W. et al. A possible buried Paleoproterozoic collisional orogen beneath central South China: Evidence from seismic-reflection profiling. *Precambrian Res.* **264**, 1–10 (2015).

Acknowledgements

The authors thank Marta Barbarano, Yaoyao Zou, Lulu Wu, and three anonymous reviewers for their insightful comments, and Carolina Ortiz Guerrero and Maria Laura Balestrieri for editorial handling. This work was supported by Natural Science Foundation of China (NSFC, No. 42372181, 42302171), the Innovation Team project of the Natural Science Foundation of Hubei Province (No. 2021CFA031) and the China Scholarship Council (CSC, No. 202106410030). No permissions were required for sampling.

Author contributions

X.Z. compiled and synthesized the data, conducted post-processing analyses, drew the figures and wrote the original draft. M.G.M developed the conceptual model, supervised the work, and reviewed and edited the final manuscript. A.R. and Q.L. contributed to data interpretation and reviewed and edited the final manuscript. Y.T. designed the field work and collected the samples. C.S. supervised the project, acquired funding, designed the field work, collected the samples, contributed to data interpretation, and reviewed and edited the final manuscript.

Competing interests

The authors declare no competing interests.

Additional information

Supplementary information The online version contains supplementary material available at https://doi.org/10.1038/s43247-025-02172-w.

Correspondence and requests for materials should be addressed to Marco G. Malusà or Chuanbo Shen.

Peer review information *Communications Earth & Environment* thanks Ni Tao, Guangwei Li and the other, anonymous, reviewer(s) for their contribution to the peer review of this work. Primary Handling Editors: Maria Laura Balestrieri and Carolina Ortiz Guerrero. [A peer review file is available].